Astron. Astrophys. 334, 585–591 (1998)

ASTRONOMY AND ASTROPHYSICS

The carbon star IRAS 06088+1909⋆

A. Richichi[1], **B. Stecklum**[2], **T.M. Herbst**[3], **P.-O. Lagage**[4], **and E. Thamm**[5]

[1] Osservatorio Astrofisico di Arcetri, Largo E. Fermi 5, I-50125 Firenze, Italy
[2] Thüringer Landessternwarte Tautenburg, Sternwarte 5, D-07778 Tautenburg, Germany
[3] Max-Planck-Institut für Astronomie, Königstuhl 17, D-69117 Heidelberg, Germany
[4] CEA, DSM/DAPNIA/Service d'Astrophysique, CE Saclay, F-91191 Gif-sur-Yvette, France
[5] Astrophysikalisches Institut und Universitäts-Sternwarte, Schillergässchen 2-3, D-07745 Jena, Germany

Received 12 June 1997 / Accepted 16 February 1998

Abstract. We present first-time investigations, by means of several different techniques in the visual and infrared domains, of the source 06088+1909, discovered by the IRAS satellite and classified as a carbon star on the basis of a SiC emission feature. Our interest for this source started with two lunar occultation events, which showed the presence of extended circumstellar emission on the scale of $\approx 0''.01$. Follow-up observations by photometry, polarimetry, spectroscopy, speckle interferometry and two more lunar occultations, have revealed many interesting characteristics, and in particular the presence of a flattened shell around the central star. By combining together all available observational evidence, we have been able to infer some of the properties of this shell, such as its shape, size, temperature of the grains, and mechanism of polarization. The object appears as one more example of the complexity existing in the environments of late-type giants and AGB stars, similar to well-known cases such as the Egg Nebula and the Red Rectangle. In the case of IRAS 06088+1909, it has been possible to conduct such a study at an unprecedented level of angular resolution.

Key words: occultations – stars: carbon – stars: circumstellar matter – stars: fundamental parameters – infrared:stars

1. Introduction

Observations capable of resolving the stellar diameter and the immediate circumstellar environment of carbon stars are particularly valuable, as they allow us to derive directly the effective temperature of the stellar atmosphere, and the characteristic size and luminosity of the shell. The direct determination of these parameters constitutes a check of fundamental importance for the theoretical models but, given the typical distances to these stars, it implies angular resolutions which are challenging. Only in very few outstanding cases, like IRC+10216 (Ridgway & Keady 1988) or IRAS 15194-5115 (Lopez et al. 1993), it has been possible to conduct useful investigations with the angular resolution delivered by diffraction-limited techniques with a single telescope, such as speckle interferometry. In general however, resolutions at the level of the millisecond of arc (mas) are needed. The options are to use long baseline interferometry (Quirrenbach et al. 1994), or lunar occultations (LO). While LO suffer from some disadvantages (first of all the fact that they only yield 1-D projections of the brightness profile), they offer very high angular resolution and are at present considerably more sensitive than interferometry at least in the infrared range. As a result, LO have produced the majority of results in this field, with about a dozen carbon stars investigated so far, as listed by Richichi et al. (1995).

In this paper, we extend the list of carbon stars for which high angular resolution observations are available, by presenting our results for IRAS 06088+1909, a very dusty carbon star toward the Galactic anticentre (Jura & Kleinmann 1990). This source was totally unknown before the IRAS observations, and was subsequently classified as a carbon star by Little-Marenin et al. (1987) on the basis of the 11.2μm SiC emission feature observed in its LRS spectrum. As such, it was included in the Stephenson's (1989) catalogue of cool galactic carbon stars, which in turn is included in our LO prediction code. When a LO of IRAS 06088+1909 was predicted to occur during one of our runs (a description of our activities in the field of LO observations can be found for instance in Richichi et al. 1996, and references therein), we were surprised to find a strong near-IR emission, since no optical counterpart was apparent at the level of the Guide Star Catalogue. Even more surprisingly, the subsequent analysis of the occultation lightcurves recorded simultaneously from two different locations showed a well resolved emission, much larger than the angular diameter expected on the basis of the observed flux and the typical photospheric temperature of a late-type star. Following this result, we obtained a series of observations with a variety of different techniques, concluded by two more LO observations. A description of the instruments and techniques employed, and of the results obtained, are given in Sects. 2 and 3. In Sect. 4, we use this observational evidence

Send offprint requests to: A. Richichi
e-mail: arichichi@arcetri.astro.it

⋆ Based on observations collected at TIRGO (Gornergrat, Switzerland), and at Calar Alto (Spain). TIRGO is operated by CNR-CAISMI Arcetri, Italy. Calar Alto is operated by the German-Spanish Astronomical Center.

Table 1. Log of the observations

Type	Date	Filter	Telescope
Occultation	25-10-94	K	CA 2.2m
Occultation	25-10-94	K	TIRGO
Photometry	26-10-94	J, H, K, L, M	TIRGO
Photom./Polarim.	15-11-94	V, R, I	CA 1.2m
Speckle	24-11-94	K, CO	CA 3.5m
Spectrum	26-11-94	K	CA 3.5m
Occultation	14-01-95	K	CA 1.2m
Occultation	14-01-95	L	TIRGO
Polarimetry	15-03-95	J, H, K	CA 3.5m
Photometry	3/5-11-96	$8-12\mu$m	TIRGO

to present a general picture of IRAS 06088+1909 and derive some of its physical characteristics.

2. Observations and data reduction

Our observations of IRAS 06088+1909 are listed in Table 1. They began with two occultations events recorded in the course of simultaneous runs at the Calar Alto and TIRGO observatories. These two sites are located at similar longitudes, but with a difference in latitude of almost 10°, which projects to ≈ 750 km at the Moon, or ≈ 40% of the Moon's radius. This ensures that a large fraction of the events observable at one site can be observed from the other one too, and along a scan angle sufficiently different to provide useful information in the case of sources that deviate from spherical symmetry, such as binary stars or circumstellar shells. The source discussed in the present paper provides an excellent example of these favourable conditions. The occultations were followed on the next day by broad-band photometry obtained at TIRGO in the 1-5μm range. After analyzing the data, and realizing the interesting characteristics of this star, further observations were stimulated, including imaging and polarimetry in the V, R, I bands, as well as speckle interferometry and low resolution spectroscopy in the near-IR, all from Calar Alto. We also succeeded in recording, in January 1995, the last occultation event of the series visible from Europe, again from both Calar Alto and TIRGO. Finally, near-IR polarimetry and thermal-IR imaging were also obtained.

Most observations were carried out using facility instruments of the two observatories, details of which are available in the literature. In particular: for the occultations and the photometry at TIRGO, the FIRT photometer was used (Richichi et al. 1996); for the visual photometry and polarimetry at Calar Alto, a CCD camera was used; for the near-IR speckle interferometry and polarimetry on Calar Alto, the MAGIC camera was used (Herbst et al. 1993). The only non-common user instrument were a) the so-called FIRPO fast IR photometer, used for the occultation events on Calar Alto: a short description of its design and its use for this kind of observations can be found in Richichi et al. (1995); and b) the CAMIRAS camera, described in Sect. 3.5.

All the filters indicated in Table 1 are standard broad-band filters, with spectral transmissions sufficiently close to the Johnson system, and it is unnecessary to report the individual characteristics. The only exception worth of mention is the L filter used at TIRGO, having λ_0=3.82μm and $\Delta\lambda$=0.64μm. The CO filter was centered at λ_0=2.295μm, with a $\Delta\lambda/\lambda\approx$1%. Details of the 8-12$\mu$m observations are reported more extensively in Sect. 3.5.

The data analysis was carried out according to the standard procedures relative to each instrument and observing mode, and we will not describe them in detail here. The only relatively non-standard techniques that we employed were those of speckle interferometry (SI) and lunar occultations (LO). In the case of SI data, a description of the data taking and processing procedures can be found in Leinert et al. (1996). In particular, the source visibility is estimated according to the classical power spectrum analysis and the phases are computed by means of the bispectrum method. In the case of LO data, we used both the well established least-squares method (LSM), and the model-independent method described by Richichi (1989, CAL hereafter). The LSM method was originally introduced in LO work by Nather & McCants (1970), however our implementation is considerably more sophisticated: a description has been given by Richichi et al. (1992). The CAL method, computationally more intensive than the LSM analysis, is necessary when it is not possible to define a priori a functional form of the brightness profile of the source. In this case, the most likely profile that satisfies the observed data within the constraints of the noise is found iteratively by modifications to a numerical profile. The method is ideally suited to derive the brightness profile of the source in case of extended circumstellar emission, and an example of the application to the case of another carbon star, namely TX Psc, can be found in Richichi et al. (1995).

3. Observational results

3.1. Lunar occultations

The LO data are shown on the left of Fig. 1, arranged to provide an intuitive overview of the different position angles of each event, and therefore of the directions along which the lunar limb scanned the source. After having inspected the data over intervals longer than those shown in the figure, having characterized the detector noise and the amount of scintillation and having carried out a preliminary analysis by the LSM method, we concluded that all the lightcurves show evidence for a well resolved central core and a surrounding extended emission. Therefore we used the CAL algorithm to derive the brightness profiles, shown in the panel to the right in Fig. 1. The result is that the profiles appear to have different characteristics along the different position angles and at the different wavelengths. One distinctive feature is that the profiles appear to be roughly symmetric about the peak, with the possible exception of the one along 124°; consider however that the signal-to-noise ratio (SNR) of the corresponding lightcurve is also the poorest among the four. Given that the range of scan angles is only 45° and that the data are not all at the same wavelength and of the same quality, it would not be justified to use tomographic techniques to obtain a 2-D image. Instead, we have attempted a simple, schematic

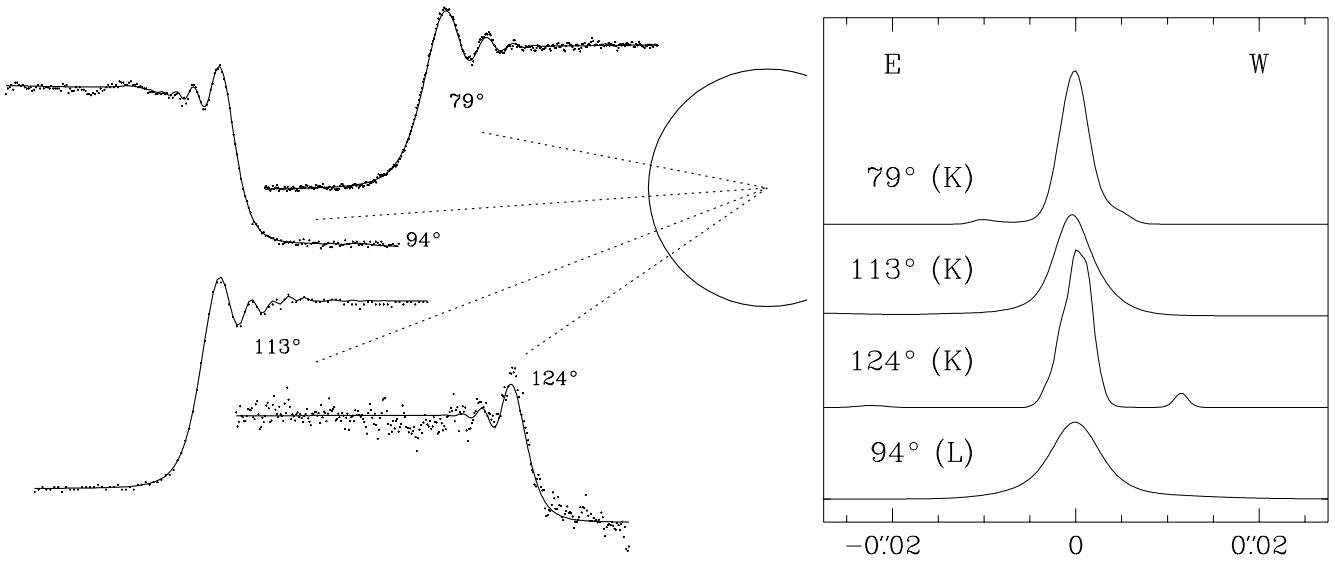

Fig. 1. Left: Data (dots) and our best fits (solid lines) for the four occultations of IRAS 06088+1909. The scan angle of each event is also indicated. From the top in counterclockwise direction, the lightcurves are those recorded at Calar Alto on 25/10/94, Tirgo on 14/01/95, Tirgo on 25/10/94 and Calar Alto on 14/01/95, respectively. For ease of presentation axes are not shown, however the typical horizontal extent covers ≈0.5 s in all cases, while the intensities on the vertical axes are in arbitrary units. Right: Brightness profiles recovered by the CAL method for the four lightcurves shown to the left. The profiles are normalized to have the same area (but note that the profile along 94° is in a different filter).

reconstruction by analyzing the two best lightcurves at 2μm in terms of a model with a central disc and an outer gaussian component. The result is that along PA=79° (113° respectively), a fraction of $85\% \pm 2\%$ of the flux ($89\% \pm 3\%$ respectively) is found to be present in a central disc with an angular diameter of 6.1 ± 0.2mas (9.3 ± 0.3mas respectively), while the remaining flux comes from the extended component which, in terms of an equivalent gaussian, has a FWHM of ≈22mas (≈40mas respectively). We note that the gaussian component is basically centered on the central disc along PA=79°, while there appears to be a significant offset, about 20mas to the East, along PA=113°. We will try to discuss these conclusions in the frame of a general picture of the source in Sect. 4. It should be noted here that this simple model analysis does not necessarily represent the only solution to the observed lightcurves; moreover, the brightness distribution of a uniform disk that we have assumed for the central component is not completely consistent with the picture that will be derived later. However, the model results derived above are largely consistent with the model-independent profiles shown in Fig. 1, and it is likely that any refinement of the model would lead only to second-order corrections which can be safely ignored in the qualitative description which will be given in Sect. 4.

3.2. Near-IR spectrum

Our K-band spectrum of IRAS 06088+1909 is shown in Fig. 2. The resolution is $\lambda/\Delta\lambda \approx 400$. In the same figure, we also show the spectrum of the CII star TU Gem, observed with the same instrument in the same night. At least a few lines are detected in the spectrum of IRAS 06088+1909, which are normally found in the atmospheres of late-type giants and AGB stars: among them those of atomic Na and Ca, and the CO band. Therefore, we tend to believe that we are detecting the photosphere, and thus the optical depth $\tau_{2\mu\mathrm{m}}$ cannot be very large. We note also that, by comparison with the spectrum of TU Gem, there is a considerable amount of veiling in IRAS 06088+1909, so that at the same time we also have to conclude that $\tau_{2\mu\mathrm{m}}$ is not very small either. Thus, the spectrum shown in Fig. 2 helps to constrain significantly the optical depth, a fact to be used in the discussion presented in Sect. 4.

3.3. Visual and near-IR photometry and polarimetry

The photometric and polarimetric characteristics of IRAS 06088+1909, measured by us in several different bands from the visual to the near-IR range, are shown in Table 2. The very red color of the source is immediately apparent (V-$K > 13$); given the distance and galactic position of the source, it is unlikely that this reddening may be caused entirely by interstellar extinction. Assuming then circumstellar dust as responsible for the extinction, it is interesting to inspect the results of polarimetry. These indicate that there might be a departure from spherical symmetry in the shell, or in general an asymmetric extinction of the light from the central source. This point will be discussed further in Sect. 4.

In addition to our determinations reported in Table 2, few other measurements are available from the literature. In particular, Epchtein et al. (1990) report the magnitudes J=9.54, H=6.93, K=4.89, L=2.32, M=1.68 (epoch 1987.2), while Noguchi et al. (1991) obtained J=8.80, H=6.40, K=4.64, L=2.25 (epoch 1989.8). It is immediately apparent that the

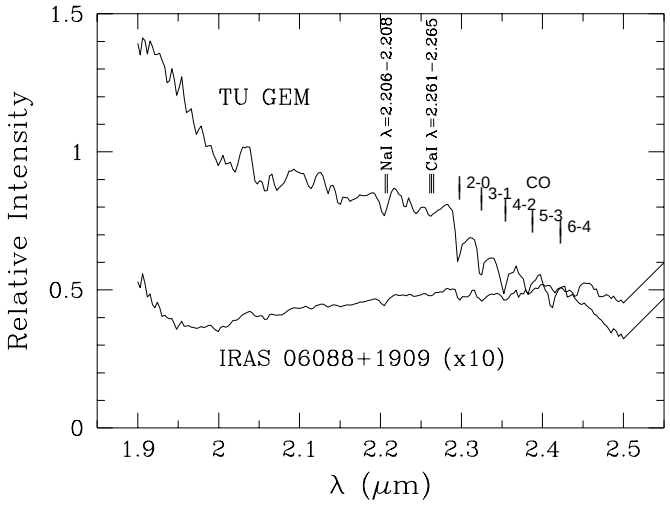

Fig. 2. K-band spectrum of IRAS 06088+1909. For comparison we also show the spectrum of the carbon star TU Gem, obtained in the same night and with the same instrument. It can be appreciated that the two spectra show essentially the same photospheric lines, but with a considerable amount of veiling in the case of IRAS 06088+1909. Notice also the very red continuum for this latter star.

Table 2. Photometry and polarimetry results

Filter	Flux	Polarization	
	(magnitude)	%	Angle
V	18.34 ± 0.12	–	–
R	14.65 ± 0.02	1.89 ± 0.12	$24\overset{\circ}{.}3 \pm 1\overset{\circ}{.}7$
I	11.29 ± 0.01	3.79 ± 0.11	$-1\overset{\circ}{.}1 \pm 0\overset{\circ}{.}8$
J	9.15 ± 0.15	5.64 ± 1.57	$5\overset{\circ}{.}0 \pm 7\overset{\circ}{.}6$
H	6.62 ± 0.02	1.86 ± 0.89	$-25\overset{\circ}{.}7 \pm 14\overset{\circ}{.}1$
K	4.61 ± 0.02	1.44 ± 0.15	$-72\overset{\circ}{.}5 \pm 5\overset{\circ}{.}2$
L	2.04 ± 0.03	–	–
	(Jy)	–	–
8.55μm	41.7 ± 2.2	–	–
9.56μm	29.9 ± 1.5	–	–
11.20μm	39.3 ± 2.0	–	–
12.45μm	27.8 ± 2.2	–	–

source is variable, a fact which is not surprising in consideration of the nature of the source. In fact, amplitudes of some tenths of a magnitude are normally found for carbon stars and late-type giants in the near-IR. It is difficult on the basis of three determinations only, to assess some kind of period, also because the variability is most likely irregular. However, we note that substantial changes in brightness probably occur also on short timescales. Our conclusion in this respect comes from an inspection of Fig. 2: the spectra of IRAS 06088+1909 and TU Gem, when integrated over the 2.0-2.4μm range, show a difference by a factor of $\approx$17.4, or $\Delta K \approx$3.1. Since TU Gem is listed in the literature has having K=1.0, we conclude that in November 1995, just one month after the photometry which yielded the value K=4.6, the magnitude of IRAS 06088+1909 was probably close to K=4.1, although this estimate is affected by some uncertainty due also to possible variations in TU Gem itself.

3.4. Speckle interferometry

Speckle interferometry measurements were carried out both in a broad band K filter and in a narrow filter centered at λ=2.295μm (this is the wavelength of the 2$\rightarrow$0 transition of CO, see also Fig. 2). The aim was: firstly, to detect the presence of extended emission on scales larger than those probed by LO; and secondly, to compare the results obtained in the "photospheric" continuum and in the CO absorption. A total of 768 frames, each with an exposure time of 0.07s, were recorded on IRAS 06088+1909 in the K band. In the narrow CO filter, the numbers were 1024 frames and 0.12s, respectively. The stars SAO 95361 and SAO 95338, both with magnitude $K \approx 5$ at a distance of $0\overset{\circ}{.}4$, were used as references for the speckle analysis, with a comparable number of frames in the two filters as the target source. The combination of exposure time, number of frames and seeing conditions ($\approx 0\overset{''}{.}7$ on average) was sufficient to allow us to reconstruct the visibility and phase in the K band with good SNR up to the diffraction limit of the 3.5 m telescope. In the narrow CO filter, the lower SNR and the longer exposure time caused some loss in the higher frequencies. We conclude that the source is effectively unresolved with an upper limit of $\approx 0\overset{''}{.}1$ for the continuum and $\approx 0\overset{''}{.}2$ for the CO band.

3.5. Thermal IR imaging

IRAS 06088+1909 was observed on November 3 and 5, 1996 at the TIRGO telescope with the Saclay CAMIRAS camera, optimised for high-angular resolution ground-based imaging in the 7.8-13.5μm atmospheric window (Lagage et al. 1992). The heart of the camera is a 192x128 Si:Ga/DVR detector array developed by the LETI/LIR of CEN Grenoble (Lucas et al. 1995). The scale was $0\overset{''}{.}72$/pixel and the total field of view was $138''$x$92''$. The aim of the observations was to derive a photometric coverage at several wavelengths in the thermal-IR to monitor possible variability (as compared to the flux measured by IRAS). Also, we wanted to investigate the structure of the source at the arcsecond level: while it was clearly unresolved in the near-IR (see the speckle results above), it was well possible that at longer wavelengths a noticeable extended emission could be detected. The source was observed in 4 different filters, having bandpasses of 8.22-8.99 μm, 9.39-9.74 μm, 10.99-11.43 μm, and 11.83-13.09 μm. The usual chopping and nodding observing technique was used to remove the huge photon background generated by the telescope and the atmosphere.

The photometry was done with α Aur, α Tau and β Gem as reference stars, which we considered as black bodies with a 10μm magnitude of -1.94, -1.24, -3.03 respectively (Tokunaga 1984). The results of the photometry as well as the 1σ statistical uncertainty are listed in Table 2 (the zero magnitude at 10μm was taken equal to 38.7Jy). The FWHM of the images was $2\overset{''}{.}3$. No significant departure between the PSF of the object and of a reference star was observed within a radius of $7\overset{''}{.}5$, and we must

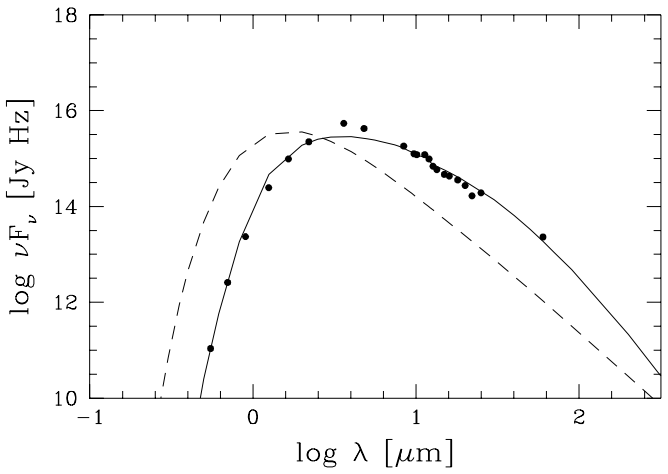

Fig. 3. Spectral energy distribution of IRAS 06088+1909. Actual data, partly from the literature and partly from our own measurements listed in Table 2, are shown as solid dots. The solid line shows our best-fit model, as explained in the text. The dashed line shows the SED of a 2200 K blackbody which is found to model the central star quite well.

conclude that IRAS 06088+1909 is effectively unresolved at the arcsecond level in the thermal-IR. We note also that the 12μm flux originally measured by IRAS was 60.2 Jy: comparing to the fluxes shown in Table 2, it appears that some variability is present even at this wavelength, as large as ≈50%. This result is interesting in itself, since in general it is expected that the amplitude of light variations in late-type stars decreases steadily with wavelength and should become very small in the thermal-IR.

4. Interpretation and discussion

At this point, several observational results already suggest the presence of circumstellar matter around IRAS 06088+1909: in fact, features such as the extended profiles measured by the LO technique, the extremely red color, the presence of a considerable amount of polarization both at visual and near-IR wavelengths would not be consistent with the simple picture of a naked stellar photosphere. Additionally, we note that Nguyen-Q-Rieu et al. (1987, NETC hereafter) detected HCN(J=1→0) emission, a feature usually considered to be a tracer of dust shells around evolved stars. Searches for emission in other tracers such as CO(J=1→0), SiC_2 and ^{29}SiO, reversely, gave negative results (NETC, Jiang et al. 1996).

Given the nature of the object, it is natural to postulate that the circumstellar shell is formed by dust ejected by the star itself. This is the first and main conclusion of this paper, and it is then appropriate to strengthen it by seeking a confirmation of the presence of dust in the spectral energy distribution (SED). This latter is shown in Fig. 3, and it clearly reveals the presence of a considerable IR excess, when compared to the emission expected from a black body with a temperature of the order of that of a cool giant star (see the dashed lined in Fig. 3).

Radiation transport calculations were performed using the one-dimensional computer model CSDUST3 of Egan et al. (1988). The code includes checks of the local and global energy conservation. Thus, the integrated fluxes under both curves in Fig. 3 are equal. The dust shell was assumed to be spherically symmetric with an inner hole. A radial density dependence of $\sim r^{-2}$ and an outflow velocity that is constant from the beginning of the flow were chosen, corresponding to the case of a constant mass-loss rate. Two types of grain composition were considered. Firstly, there should exist pure carbon particles around the C-rich star. For the opacities, we took the data from Preibisch et al. (1993) for amorphous carbon. A second grain type containing silicon was also assumed. These particles have a mantle of carbon around a SiC core. The core-mantle volume ratio is 1:1. Both grain types were modeled as homogenous spheres with a radius of 50 nm. The major parameters used in the radiative transfer calculations are listed in Table 3.

Table 3. Parameters of the radiative transfer model

Star	Effective temperature $T_{\rm eff}$	2200 K
	Luminosity L	10^4 $L_\odot$
	Distance d	2500 pc
	Angular diameter ϕ_*	2.6 mas
Circumstellar shell	Inner radius r_i	3×10^{12} m
	Outer radius r_o	5.4×10^{14} m
	Temperature T(r_i)	990 K
	Temperature T(r_o)	100 K
	Total mass M	6.3×10^{-3} $M_\odot$

These assumptions are of course preliminary, and it would be necessary to run more refined models in order to describe more carefully the dust properties and expecially the geometry of the shell. However the results obtained even in this simple approximation are consistent with the rest of our conclusions and we consider it useful to list them. In particular, our model gives an effective temperature of the central star of ≈2200 K, and a distance of 2500 pc. We note that the distance to IRAS 06088+1909 derived by this model is consistent with the results of Loup et al. (1993). At this point, it is not possible to obtain an independent distance indicator for this source, and we have to limit ourselves to the conclusion that, over the luminosity range 7×10^3 to 2×10^4 $L_\odot$ (typical for this kind of stars) a consistent fit to the SED can be achieved using a distance in the range 2 to 3.5 kpc. We note that the LSR velocity of the HCN line measured by NETC, if interpreted as due to galactic rotation, would imply a distance >25 kpc: this would lead in turn to a very high luminosity and should probably be ruled out. The angular diameter from our model is $\phi_* = 2.6$ mas, which is smaller by a factor of ≈2-3 than the size of the central core of the brightness profiles derived the LO: this shows that the stellar photosphere is not dominating at λ=2.2μm, although the difference is not very large and therefore also the optical depth cannot be very large. The visual extinction required to fit the SED is $A_V = 6.7$ mag: this cannot be explained by interstellar extinction only, which in this direction at a distance of 2.5kpc is expected to be between 0.5 and 1.0 mag (Lucke 1978). The circumstellar shell extends from $r_i \approx 20$ AU to $r_o \approx 3600$ AU. The inner radius is about 6 times the stellar radius,

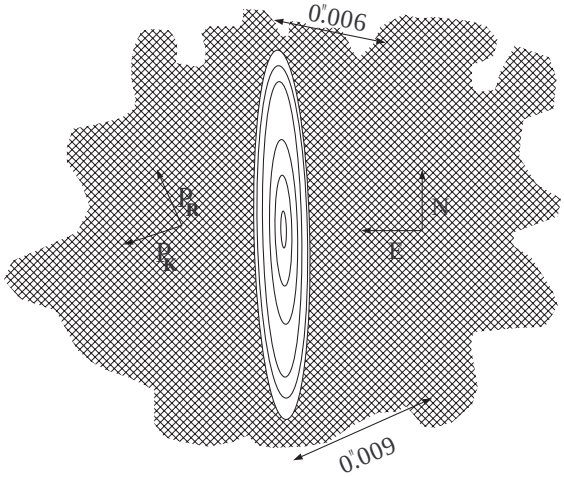

Fig. 4. Schematic reconstruction of the structure observed at the milliarcsecond scale in the K band, from the LO data discussed in Sect. 3.1. The central elongated component is responsible for $\approx 85\%$ of the emission at 2μm. The vectors P_R and P_K indicate the direction of the linear polarization observed in these two bands, as listed in Table 2. The segments with extension of 6 and 9 mas represent the projected extent and orientation of the shell as measured by the LO events.

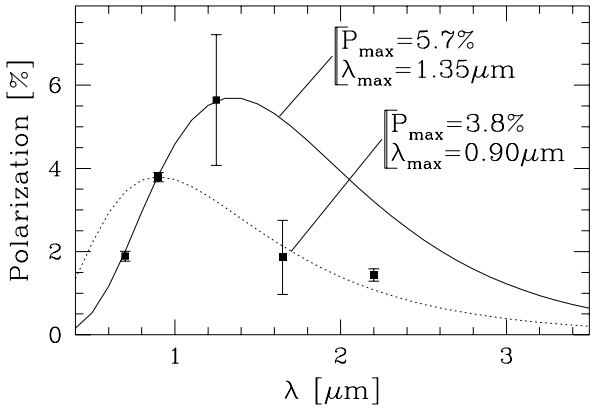

Fig. 5. Plot of the polarization data of Table 2; also shown are two models based on the Serkowski law (1973) with the parameters shown.

i.e. the dust-free zone has an angular diameter of $\approx$ 16 mas. The grain temperatures at the inner radius of the dust shell are found to be ≈990K, and ≈100K at the outer radius. We note that a simple fit to the SED by means of two black bodies was computed also by NETC, leading to temperatures of 950K and 400K for the hot and cold components.

We now try to estimate more quantitatively some characteristics of the circumstellar component, and we begin with the issue of its geometrical appearance. To this purpose, we use the LO results described in Sect. 3.1; in particular, the analysis in terms of a two-component model leads us to draw the simple sketch shown in Fig. 4, with an elongated central core having a size $\approx 0\farcs02$ along its major axis, and emitting $\approx 85\%$ of the 2μm flux; this is surrounded by a more extended emission on scales of $\gtrsim 0\farcs04$, with a rather low contrast, and that we show only partially as a fuzzy background in Fig. 4. The central component appears to be flattened and oriented along PA$= 2^\circ$: this is derived from the projections measured along two different angles by the LO scans. The minor axis of this flattened central component has a size of $\lesssim$ 3mas: it is interesting to note that this is very close to the value of the stellar diameter derived above by a simple analysis of the SED.

The next step is to explain the polarization results listed in Table 2. In this respect, we note firstly that the wavelength dependence of the polarization degree cannot be easily fitted by a simple Serkowski law, as shown in Fig. 5. As a result, we can rule out dichroic extinction as mechanism for the observed polarization; furthermore, it would be hard to justify in a carbon star the strength of the magnetic field required to produce an adequate alignment of the grains. Scattering is then the next likely possibility as a polarization mechanism, and the question arises whether it is possible to think of a geometry that a) could produce the observed large changes in the polarization angle with wavelength, and b) could be consistent with the LO results.

The answer is positive, if one postulates that the elongated structure seen in Fig. 4 is optically thick at visual wavelengths, but becomes progressively thinner at longer wavelengths. This kind of geometry has been invoked already to explain observations of young stars with a considerable amount of circumstellar matter in the shape of a disk or flattened shell (see for instance Tamura & Sato, 1989). In this case, light at the shorter wavelengths is completely absorbed in the plane of the disk, but can escape along the direction of its axis and is then scattered by the material above and below the disk. If one assumes that this material is optically thin, visual light can escape in the direction to the observer with a single scattering. Computations show that the net result (our polarization measurements of course do not resolve neither the central core nor the more extended, fainter structure) is that the light will be polarized mainly parallel to the disk. In the near-IR, one could assume that the disk has decreased its optical thickness to such a level that single-scattering photons can reach the observer directly from the disk (which would also be the main source of polarization, since the outer material would be too thin to produce significant scattering). In this case, the net polarization would be perpendicular to the disk itself.

This explanation seems to fit the sketch shown in Fig. 4 quite convincingly: in fact, the central structure that we infer from the LO data is very flattened, and for all purposes can be seen as some kind of disk. Also, the polarization directions observed at R and K lie almost exactly at 90° to each other as predicted in the model above, and the K polarization is aligned within $\approx 15^\circ$ of the expected direction. It remains to be proven that this "disk" is effectively optically thick in the visual, and optically thin in the near-IR. One first argument in favor of this comes from the SED shown in Fig. 3: there can be little doubt that the visual light is indeed extincted, and we estmated that $A_V \approx 6$ mag. We also concluded that, on the basis of the near-IR spectrum and of the model fitting the SED, along the line of sight to the star we cannot have $\tau_{2\mu m} \gg 1$. On the other hand,

we can estimate that assuming a standard law of the wavelength dependence of extinction in an interstellar environment (see for instance Natta & Panagia 1984), the infrared extinction is relatively small, $A_K \approx 0.5$ mag.

It is more difficult to estimate whether the necessary conditions are met also for the outer, thinner component, i.e. that it give rise to single scattering for visual light and negligible scattering for the near-IR. However, we note that the ratio of the emission density of the inner and outer components is $\approx 10^2$ at 2μm (from LO results), and at least qualitatively this would justify the required assumptions.

5. Summary and concluding remarks

We have obtained first-time measurements of the carbon star IRAS 06088+1909 using a variety of techniques, namely: lunar occultations at several wavelengths and along several scan angles; visual, near-infrared and thermal infrared imaging and photometry; visual and infrared polarimetry; an infrared spectrum; and infrared speckle interferometry. This wealth of information has revealed an interesting object, whose characteristics include very red colors, variability, a strong circumstellar extinction and peculiar polarization; it is well resolved spatially by the lunar occultations measurements, which show a flattened central core with a characteristic size of $\approx 0''.02 \times 0''.003$, surrounded by a more extended, tenuous emission.

All this observational evidence has been put together, to obtain a consistent picture of a central luminous carbon star surrounded by a dust shell which appears considerably flattened, to the point that it can be considered similar to a disk. The major axis of this disk has an extent that corresponds to $\gtrsim$50AU at an estimated distance of $\gtrsim$2.5kpc. The minor axis is comparable to the stellar diameter. The dust temperature is close to 1000K at the inner edge. The disk is oriented approximately in a North-South direction, and its geometry explains the observed polarization both at visual and near-IR wavelengths.

It is almost natural to compare IRAS 06088+1909 with outstanding objects such as the Egg Nebula or the Red Rectangle, which are well known examples of late-type stars at the end of their evolution, surrounded by dust with interesting characteristics and geometries (Sahai et al. 1995, Roddier et al. 1995). The interest in the case of IRAS 06088+1909 lies in the fact that for the first time it has been possible to study such dust features at a scale of few milliseconds of arc, a feat made possible by the use of lunar occultations. For comparison, this scale is more than on order of magnitude smaller than that allowed by the HST at visual wavelengths, or by the largest ground-based telescopes in the near-IR. One can think of IRAS 06088+1909 as an excellent target for the near-future, when a generation of facilities will come into operation (including the Keck and VLT interferometers and the LBT) which will fulfill for the first time the necessary requirements of baselines and sensitivity.

Acknowledgements. This work has been made possible by friends and colleagues, which have helped us during observations or with useful discussions: our thanks go to G. Calamai, O. Fischer, F. Lisi, A. Natta, H.G. Reimann. This research has made use of the *Simbad* database, operated at CDS, Strasbourg (France). A.R. has been partially supported in his work by a Chretien Grant awarded by the American Astronomical Society. B.S. acknowledges support from DFG grants for performing observations at Calar Alto.

References

Egan M.P., Leung C.M., Spagna G.F. 1988, Computer Phys. Comm. 48, 271
Epchtein N., Le Bertre T., Lépine T. 1990, A&AS 227, 82
Herbst T.M., Beckwith S.V.W., Birk Ch., et al. 1993, SPIE Conference 1946, 605
Jiang B.W., Deguchi S., Yamamura I., et al. 1996, ApJS 106, 463
Jura M., Kleinmann S.G. 1990, ApJ 364, 663
Lagage P.O. et al. , 1992, in *42nd ESO Conference*, ed. Ulrich M.H., 601
Leinert Ch., Richichi A., Haas M. 1996, A&A 318, 472
Little-Marenin I.R., Ramsay M.E., Stephenson C.B., Little S.J., Price S.D. 1987, AJ 93, 663
Lopez B., Perrier C., Mékarnia D., Lefévre J., Gay J. 1993, A&A 270, 462
Loup C., Forveille T., Omont A., Paul J.F. 1993, A&AS 99, 291
Lucas C., Bischoff I., Chammings G., et al. 1995, SPIE Conference 2475, 50
Lucke P.B. 1978, A&A 64, 367
Nather R.E., McCants M.M. 1970, AJ 75, 963
Natta A., Panagia N. 1984, ApJ 287, 228
Noguchi K., Sun J., Wang G. 1991, PASJ 43, 275
Nguyen-Q-Rieu, Epchtein N., Truong-Bach, Cohen M. (NETC) 1987, A&A 180, 117
Preibisch Th. Ossenkopf V., Yorke H.W., Henning Th. 1993, A&A 279, 577
Quirrenbach A., Mozurkevich D., Hummel C.A., Buscher D.F., Armstrong J.T. 1994, A&A 285, 541
Richichi A. 1989, A&A 226, 366
Richichi A., Di Giacomo A., Lisi F., Calamai G. 1992, A&A 265, 535
Richichi A., Chandrasekhar T., Lisi F., et al. 1995, A&A 301, 439
Richichi A., Baffa C., Calamai G., Lisi F. 1996, AJ 112, 2786
Ridgway S.T., Keady J.J. 1988, ApJ 326, 843
Roddier F., Roddier C., Graves J.E., Northcott M.J. 1995, ApJ 443, 249
Sahai R., Trauger J.T., Evans R.W., et al. 1995, BAAS 187, 4403
Serkowski K. 1973, IAU Symp. 52, Greenberg J.M., van den Hulst H.C. (eds.), Reidel, Dordrecht, 145
Stephenson C.B. 1989, Publ. Warner & Swasey Obs. 3, no. 2
Tamura M., Sato S. 1989, AJ 98, 1368
Tokunaga A. 1984, AJ 89, 172